

Article

Performance Improvement Using ICIC for UAV-Assisted Public Safety Networks with Clustered Users during Emergency

Abhaykumar Kumbhar 

Motorola Solutions, Inc., Plantation, FL 33322, USA; abhaykumar.kumbhar@gmail.com

Abstract: The application of drones, also known as unmanned aerial vehicles deployed as unmanned aerial base stations (UABSs), has received extensive interest for public safety communications (PSC) to fill the coverage gaps and establish ubiquitous connectivity. In this article, we design a PSC LTE-Advanced air-ground-based HetNet (AG-HetNet) that is a scenario representation of a geographical area during and after a disaster. As part of the AG-HetNet infrastructure, we have UABSs and ground user equipment (GUE) flocking together in clusters at safe places or evacuation shelters. AG-HetNet uses cell range expansion (CRE), intercell interference coordination (ICIC), and 3D beamforming techniques to ensure ubiquitous connectivity. Through system-level simulations and using a brute-force technique, we evaluate the performance of the AG-HetNet in terms of fifth-percentile spectral efficiency (5pSE) and coverage probability. We compare system-wide 5pSE and coverage probability when UABSs are deployed on a hexagonal grid and for different clustering distributions of GUEs. The results show that reduced power subframes (FeICIC) defined in 3GPP Release-11 can provide practical gains in 5pSE and coverage probability than the 3GPP Release-10 with almost blank subframes (eICIC).

Keywords: cell range expansion; clustered users; eICIC; FeICIC; FirstNet; interference management; Matérn cluster process; public safety; Thomas cluster process; UAV



Citation: Kumbhar, A. Performance Improvement Using ICIC for UAV-Assisted Public Safety Networks with Clustered Users during Emergency. *Telecom* **2023**, *4*, 816–835. <https://doi.org/10.3390/telecom4040036>

Academic Editor: Sotirios K. Goudos

Received: 27 June 2023

Revised: 3 August 2023

Accepted: 7 November 2023

Published: 20 November 2023



Copyright: © 2023 by the author. Licensee MDPI, Basel, Switzerland. This article is an open access article distributed under the terms and conditions of the Creative Commons Attribution (CC BY) license (<https://creativecommons.org/licenses/by/4.0/>).

1. Introduction

Unmanned aerial base stations (UABSs)-based communications and networking provide deployment flexibility in three-dimensional (3D) space and enable ubiquitous and non-line-of-sight (NLOS) connectivity. More specifically, UABS are deployed to meet mobile data and coverage needs. Furthermore, by restoring any damaged infrastructure and relieving the pressure on the terrestrial networks, it reduces the cost of dense small cell deployments [1–5]. During one such emergency, AT&T deployed a cell-on-wings (COW) drone to restore Long Term Evolution (LTE) cell coverage in Puerto Rico [6–8] in the aftermath of Hurricane Maria. This application demonstrates the capability of UABSs to support mission-critical communication and enables high-speed real-time data, video, and multimedia services.

A challenge while designing an LTE-Advanced public safety communications (PSC) network is to ensure seamless and ubiquitous coverage. Especially during and after an emergency, trying to achieve the ubiquitous broadband coverage criteria would be difficult, using only the limited terrestrial infrastructure. One of the main design criteria for a PSC network, such as the first responder's network authority (FirstNet) in the United States, is to attain at least a 95% coverage of the geographical area and human population enabled with broadband rates [9]. Another critical aspect during and after an emergency is that the general public (civilian cellular users) tends to cluster at various safe and secure locations. However, this clustering of users could lead to network congestion over the limited terrestrial network in the region. To this end, several academic research articles have focused on investigating the role of UABSs in improving spectral efficiency (SE) and wireless coverage in [4,5,10–19].

1.1. Literature Review

The past literature and ongoing research have primarily focused on specific aspects of UABS-based communications rather than considering all elements of the air-ground HetNet (AG-HetNet) and the wireless network as a whole. In particular, taking into account the distribution of users in the post-disaster scenario, such as after a hurricane or earthquake. In a post-disaster scenario, civilians and first responders gather at safe shelters, leading to localized clustering of users at specific locations within the AG-HetNet. To this end, the role of UAVs as UABSs has been explored to provide LTE-Advance/5G services to civilians and first responders. However, the deployment of UABSs tends to introduce inter-cell interference with the existing infrastructure. In this section, we investigate the primary focus of the past literature and ongoing research and compare the findings to the contributions in this article.

In particular, refs. [10,15,18,20] have analyzed the performance of unmanned aerial vehicle (UAV)-assisted cellular networks with clustered users using a stochastic framework. A UAV-based ad hoc network was proposed in [10,15,20] to improve the overall performance of the network and enhance user experience in terms of throughput, coverage, and energy efficiency, respectively. In [18], a statistical framework was proposed where users in a post-disaster scenario are modeled using the traditional Matern and Thomas cluster process. Furthermore, numerical analysis and Monte Carlo simulation are considered to verify the find closed-form expressions, which quantified the performance and gains in terms of coverage probability, spectral efficiency, and energy efficiency of the user downlink. However, during the investigation and performance analysis, the authors did not consider the significance of the 3GPP Release-10 and Release-11 ICIC techniques for the AG-HetNet deployments. Similar extensive studies to evaluate UAV-based ad hoc PSC have been conducted in [21–24]. The wireless network model under investigation focused on optimizing limited aspects such as coverage, interference analysis, resource optimization, and user scheduling using suitable heuristic approaches. However, the authors did not consider the AG-HetNet scenario with the inclusion of 3GPP-defined ICIC and positive-bias cell range expansion techniques.

The 3GPP Release-10 and Release-11 ICIC techniques have been studied in [25–27] for HetNets. For example, ref. [25] proposes algorithms that jointly optimize the inter-cell interference parameters, association rules for ground users in HetNet, and the spectrum resources shared between the terrestrial macro and small cells. However, the 3GPP Release-11 FeICIC technique for better radio resource utilization and positive bias range expansion at small cells for offloading a larger number of ground users to small cells was not considered in [25]. Nevertheless, refs. [25–27] do not consider UABSs nor address any UABS integration issues into an existing HetNet.

With AG-HetNet under consideration in articles [4,5,17,28,29], the effectiveness of the 3GPP Release-10 enhanced ICIC (eICIC) and Release-11 further-enhanced ICIC (FeICIC) techniques were investigated. In particular, the effectiveness of the 3GPP Release-10 enhanced ICIC (eICIC) and Release-11 further-enhanced ICIC (FeICIC) techniques while taking positive bias cell range expansion (CRE) at UABS was taken into account and has been studied in [4,5,17,28]. The authors in these articles have considered a similar approach to the system model and considered various meta-heuristic algorithms to address challenges of interference mitigation and jointly optimize resource block scheduling, positive bias CRE, and the UAV locations to achieve mission-critical coverage and throughput. Whereas, in [29], the authors compared the performance of interference management for PSC for the eICIC, FeICIC, and coordinated multipoint for the coordinated scheduling technique using a deep learning-based approach. However, these articles do not consider the effects of clustered users, such as overloading and congestion, only at specific base stations in the AG-HetNet.

1.2. Contributions

This initial investigation considers a PSC scenario setup in an urban environment with fixed MBS and mobile UABSs constituting an AG-HetNet infrastructure operating in the LTE band class 14 frequency [2]. Each base station in the AG-HetNet model proposed in Section 2 is integrated with three-dimensional (3D) beamforming (3DBF). In specifics, the macro base stations (MBSs) can use inter-cell interference coordination (ICIC) techniques defined in 3GPP Release-10/11 and UABSs can utilize cell range expansion bias (CRE) defined in 3GPP Release-8 to offload ground user equipment (GUE) from MBSs.

Within the defined AG-HetNet, a mock emergency scenario is simulated by randomly eliminating several fixed MBSs and the GUEs clustering at locations irrespective of cellular coverage and infrastructure as shown in Figure 1. During or in the aftermath of an emergency, the UABS are deployed on a fixed hexagonal grid to restore damaged infrastructure and relieve the network congestion on the terrestrial networks. Subsequently, to evaluate the performance of this AG-HetNet, we consider *coverage probability* and *fifth percentile SE (5pSE)* as the key performance indicators (KPIs). To maximize these two KPIs of the wireless network, we optimize the ICIC and CRE network parameters using a brute-force technique while mitigating intercell interference. Our specific contributions and comparison with the existing literature are summarized in Table 1. To summarize the key contributions of this article,

- We first define a framework for the AG-HetNet public safety network that considers a real-life disaster event, such as hurricanes or earthquakes, and the potential impact on public safety infrastructure and real-time users.
- To accurately study the signal reliability and performance improvement for the PSC in the disaster-struck, public safety network, the system model considers several key aspects, such as the CRE, ICIC, and 3DBF defined in various 3GPP releases.
- In the disaster-struck, public safety network, we evaluate and analyze the performance of AG-HetNet for different ICIC schemes and different numbers of UABS deployments.

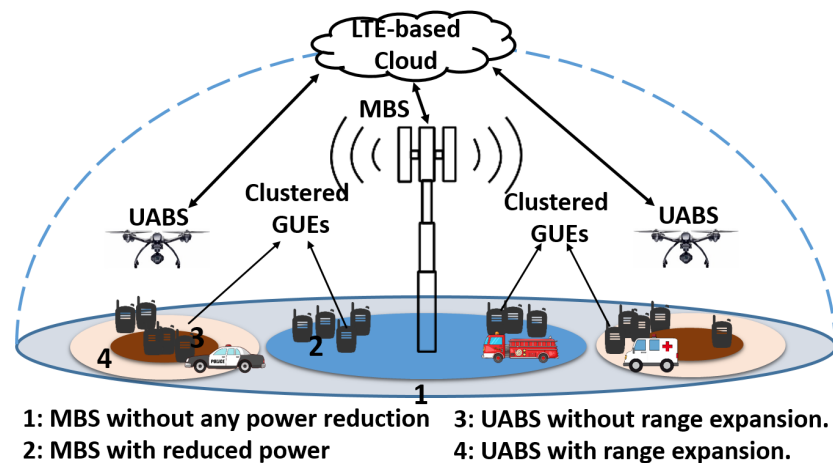


Figure 1. An illustration of a PSC scenario with fixed MBS, mobile UABSs, and clustered GUEs constitute the air-ground HetNet infrastructure. The MBS can use various inter-cell interference coordination techniques defined in LTE-Advanced. The UABSs can utilize range expansion bias to offload GUEs from MBS.

Table 1. Literature review on whether clustered users were considered and type of distributions used for modeling the user clusters, optimization techniques used, and the optimization goals of the system model.

Ref.	Cluster	User Distribution	Optimization Techniques	Optimization Goals
[30]	✗	✗	Swarm intelligence algorithms	resource scheduling, parameter optimization
[31]	✗	✗	Fuzzy C-means	resources optimization, path planning
[29]	✗	Equitably & randomly	Deep learning	interference coordination
[23]	✗	Randomly	Reinforcement learning	network coverage, optimal UAV placement
[21]	✗	Uniformly	Numerical	coverage, interference coordination
[5]	✗	Poisson point process (PPP)	Brute-Force, Genetic Algorithm	spectral efficiency, energy efficiency, interference coordination
[4]	✗	PPP	Brute-Force, eHSGA, Genetic Algorithm	spectral efficiency, energy efficiency, interference coordination
[32]	✗	PPP	Brute-Force, Genetic approach	spectral efficiency, coverage
[17]	✗	PPP	Q-learning, Deep Q-learning, Brute-force, Sequential algorithm	spectral efficiency, energy efficiency, interference coordination
[20]	✓	Fast K-means	Numerical	power optimization, resource allocation
[15]	✓	Poisson cluster process (PCP)	Stochastic geometry	coverage probability and downlink analysis
[33]	✓	TCP	Closed-form bounds	CDF of the nearest neighbor and contact distance distributions of clusters
[34]	✓	MCP	Closed-form bounds	CDF of the nearest neighbor and contact distance distributions of clusters
[35]	✓	PCP	Stochastic geometry to find correlation between base-station cell locations	resource block management, coverage probability, throughput
[36]	✓	PPP, PCP	Geometry-based analysis	downlink coverage probability, interference coordination
Our Work	✓	TCP and MCP	Brute-Force	spectral efficiency, energy efficiency, interference coordination

The rest of this paper is organized to define AG-HetNet, the wireless network parameters, and the performance evaluation in various sections. In Section 2, an LTE-Advanced AG-HetNet system is defined, where each base station is integrated with 3DBF and the determined KPIs are expressed as a function of network parameters. The UABS fixed deployment scheme and ICIC network parameter optimization using a brute-force technique are described in Section 3. Whereas in Section 4, via extensive computer-based simulations, we analyze and compare the defined KPIs of the AG-HetNet for various ICIC techniques and clustering distributions of GUE. Finally, the last section provides concluding remarks. Table 2 lists the notations and symbols used throughout the paper.

Table 2. Notations and symbols used in the system model.

Symbol	Description
$\mathbf{L}_{mbs}^{3D}, \mathbf{L}_{ue}$	Locations of MBS and UE.
$\Lambda_{mbs}, \Lambda_{gue}$	Distribution intensities of the MBS and UE nodes
Pow_{mbs}, Pow_{uabs}	Maximum transmit power of MBS and UABS
$A_E(\phi, \theta)$	Transmitter antenna's 3DBF element of antennas for all base stations
F	Account for Nakagami fading
$\varphi(d_{on}), \varphi(d_{un})$	Respective path loss from MBS and UABS in dB

Table 2. Cont.

Symbol	Description
f_c^{B14}	Carrier frequency in PSC band 14
h_{bs}	Altitude of the base station in Okumura–Hata model
h_{mbs}, h_{uabs}	Altitude of MBS and UABS
h_{gue}	Altitude of a UE in Okumura–Hata model
d_{mn}, d_{mu}	UE distance from MOI and UOI
$Pow'_{mbs}(d_{on})$	RSRP from MOI
$Pow'_{uabs}(d_{un})$	RSRP from UOI
I_{agg}	Aggregate interference at GUE from all base stations, except MOI/UOI
$\Gamma_{usf}^{mbs}, \Gamma_{usf}^{uabs}$	SIR from MOI and UOI in USF subframes
$\Gamma_{usf}^{mbs}, \Gamma_{usf}^{uabs}$	SIR from MOI and UOI in CSF subframes
α_{mbs}	MBS Power reduction factor during CSF transmission
β_{mbs}	Duty cycle for USF transmission
τ_{uabs}	Cell range expansion bias
ρ_{mbs}, ρ_{uabs}	Scheduling threshold for MUE and UUE
$N_{usf}^{mbs}, N_{csf}^{mbs}$	Number of USF-MUEs and CSF-MUEs
$N_{usf}^{uabs}, N_{csf}^{uabs}$	Number of USF-UUEs and CSF-UUEs
$C_{usf}^{mbs}, C_{csf}^{mbs}$	Aggregate SEs for USF-MUEs and CSF-MUEs
$C_{usf}^{uabs}, C_{csf}^{uabs}$	Aggregate SEs for USF-UUEs and CSF-UUEs
$\hat{\mathbf{l}}^{(hex)}$	Fixed hexagonal locations of deployed UABS
\mathbf{S}_{mbs}^{ICIC}	Matrix representation of ICIC parameters for MBSs
\mathbf{S}_{uabs}^{ICIC}	Matrix representation of ICIC parameters for UABSs
\mathbf{rad}	Radius of the Matern Cluster Process
AR_{sim}	Simulation area

2. System Model

This article considers an AG-HetNet before and after a disaster, as shown in Figure 2. In particular, Figure 2a shows a typical public safety network with most of the geographical area under broadband coverage before a disaster. In a disaster, the public safety network infrastructure is destroyed and the first responders and victim users experience an SE outage, as illustrated by the white areas in Figure 2b. Furthermore, Figure 2b also illustrates that GUEs are clustered at locations irrespective of the cellular coverage and infrastructure.

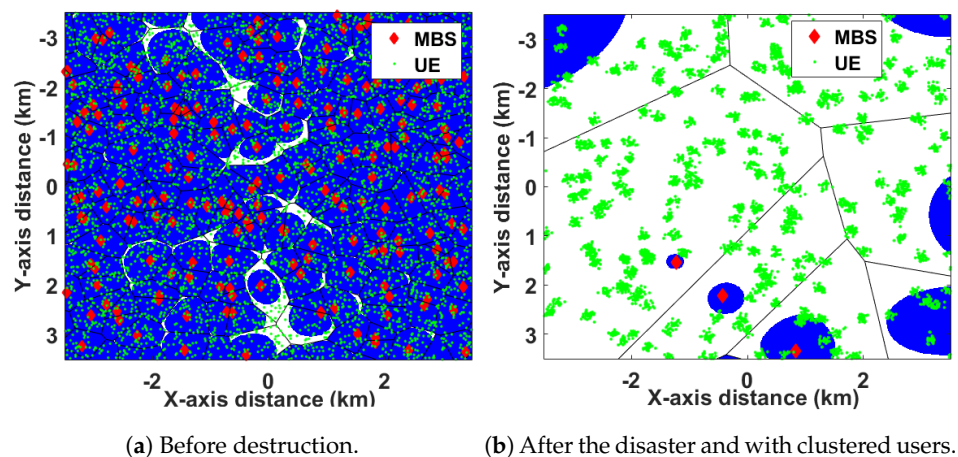


Figure 2. Illustration of Typical PSC AG-HetNet and SE coverage before/after a disaster.

To simulate the public safety scenario, a two-tier AG-HetNet is modeled, with 3D locations of MBS and UABS captured in matrices $\mathbf{L}_{mbs}^{3D} \in \mathbb{R}^{N_{mbs} \times 3}$ and $\mathbf{L}_{uabs}^{3D} \in \mathbb{R}^{N_{uabs} \times 3}$, respectively, with N_{mbs} and N_{uabs} denoting the number of MBSs and UABSs within the simulation area (AR_{sim}). Similarly, the 3D distribution of GUEs is captured in matrices \mathbf{L}_{gue} with a density of Λ_{gue} and modeled using the Matérn cluster process (MCP) and Thomas

cluster process (TCP). Wherein MCP and TCP are the special cases of the Neyman–Scott process [37],

- MCP: To simulate the MCP distribution, we assume a homogeneous Poisson point process with an intensity Λ_{gue} within the AR_{sim} . For each point of the underlying point process, a Poisson number of points is simulated with mean $\mu > 0$ and distributed uniformly on a disk with a constant radius $\mathbf{rad} > 0$. The considered underlying point process is also called the parent (point) process and its points are the centers of the cluster disks. The subsequent point process on all the disks is called the daughter (point) process and is responsible for forming the clusters.
- TCP: To simulate the TCP distribution, we again assume a homogeneous Poisson point process with an intensity Λ_{gue} within AR_{sim} . For each point of the underlying point process, a Poisson number of points with mean $\mu > 0$, we simulate two independent zero-mean normal variables with a variance σ^2 corresponding to the Cartesian coordinates. The considered underlying point process is also called the parent (point) process and its points are the centers of the cluster disks. The subsequent point process on all the disks is called the daughter (point) process and each daughter point is scattered around the origin based on a normal distribution with variance σ^2 .

In the assumed public safety scenario, N_{gue} are the total number of GUEs scheduled in AG-HetNet. Consider an arbitrary GUE n , such that the nearest distance from any macrocell of interest (MOI) and UABS' cell of interest (UOI) is given by d_{on} and d_{un} , respectively. With a fixed antenna height, the location of wireless node MBS is modeled using a 2D Poisson point process (PPP) with densities Λ_{mbs} . On the other hand, UABS is deployed on a fixed hexagonal grid at a fixed altitude. The densities and deployment heights of each wireless node in the AG-HetNet under consideration are specified in the Table defined in Section 4. Finally, assuming a Nakagami- m fading channel, the reference symbol received power from UOI and MOI can be given as

$$\begin{aligned} \text{Pow}'_{\text{uabs}}(d_{un}) &= \frac{\text{Pow}_{\text{uabs}} A_{3\text{DBF}}(\phi, \theta) F}{10^{\varphi(d_{un})/10}}, \\ \text{Pow}'_{\text{mbs}}(d_{on}) &= \frac{\text{Pow}_{\text{mbs}} A_{3\text{DBF}}(\phi, \theta) F}{10^{\varphi(d_{on})/10}}, \end{aligned} \quad (1)$$

where the variables $\varphi(d_{on})$ and $\varphi(d_{un})$ are the path loss, respectively, observed from MBS and UABS in dB. Additionally, the random variable F accounts for Nakagami- m fading, whose probability density function is given by [4]

$$f_N(\psi, w) = \frac{w^w \psi^w}{\Gamma(w)} \exp(-w\psi), \quad (2)$$

where w is the shaping parameter, ψ is the channel amplitude, and $\Gamma(w)$ is the standard Gamma function given as $\Gamma(w) = \int_0^\infty \exp(-u) u^{w-1} du$. Through the shaping parameter w , the received signal power can be approximated to variable fading conditions. The value $w > 1$ approximates to Rician fading along line-of-sight (LOS) and $w = 1$ approximates to Rayleigh fading along NLOS.

In Equation (1), we define $A_{3\text{DBF}}(\phi, \theta)$ as the transmitter antenna's 3DBF element, where θ and ϕ is the zenith and azimuth of the spherical angles and unit vectors. By restating the definition of $A_{3\text{DBF}}(\phi, \theta)$ given in [4,38], the equation is as follows

$$\begin{aligned} A_{3\text{DBF}}(\phi, \theta) &= G_{3\text{DBF,max}} - \min \{ - (A_{\text{Hor}}(\phi) + A_{\text{Ver}}(\theta)), A_m \}, \\ G_{3\text{DBF,max}} &= 8 \text{ dBi}, A_m = 30 \text{ dB}, \end{aligned} \quad (3)$$

where $A_{\text{Hor}}(\phi)$ is the antenna horizontal element, whereas $A_{\text{Ver}}(\theta)$ is the antenna vertical element of the radiation pattern and is given by

$$A_{\text{Hor}}(\phi) = -\min \left[12 \left(\frac{\phi}{\phi_{3\text{dB}}} \right)^2, A_m \right], \phi_{3\text{dB}} = 65^\circ, \quad (4)$$

$$A_{\text{Ver}}(\theta) = -\min \left[12 \left(\frac{\theta - \theta_{\text{tilt}}}{\theta_{3\text{dB}}} \right)^2, SLAV \right], \theta_{\text{tilt}} = 90^\circ, \quad (5)$$

$$SLAV = 30, \theta_{3\text{dB}} = 65^\circ.$$

3DBF can further assist the interference coordination process and has the potential to significantly improve the signal-to-interference ratio (SIR) of the desired signal by calibrating MBS ($P_{\text{ow}_{\text{mbs}}}$) and UABS ($P_{\text{ow}_{\text{uabs}}}$) [39]. Thus, by regulating the transmission power, we achieve significant improvements to SIR for the GUEs located at the cell edge or the GUEs in the range-expanded regions. Furthermore, this technique also helps to check the power transmitted into the neighboring cell sites.

2.1. Path Loss Model

To accurately study the signal reliability for the PSC in an urban environment, well-defined air-to-ground and ground-to-ground communication links are considered between the interfacing base station of interest (BOI) and the GUEs available. To this end, we consider Okumura–Hata Path Loss (OHPL) models for accurate analysis of signal reliability for the proposed AG-HetNet, especially in an urban terrestrial environment where the base station height does not vary and OHPL is an optimal path model [5]. When a GUE camps on a base station of interest (MOI or UOI), OHPL for the AG-HetNet is given by

$$\varphi(d) = 74.52 + 26.16 \log(f_c^{\text{B14}}) - 20.37 \log(h_{\text{bs}}) - 3.2(\log(11.75 h_{\text{gue}}))^2 + 38.35 \log(d), \quad (6)$$

where f_c^{B14} is the carrier frequency in MHz and h_{bs} is the height of MBS, i.e., $h_{\text{bs}} = h_{\text{mbs}}$, h_{gue} is the height of GUEs in meters, and h_{uabs} is the height of UABSs in meters.

Figure 3 characterizes the empirical path loss cumulative distribution functions (CDFs) for the OHPL model, calculated for all distances between the base stations ($\mathbf{L}_{\text{mbs}}^{\text{3D}}$ and the $\mathbf{L}_{\text{uabs}}^{\text{3D}}$) and GUEs (\mathbf{L}_{gue}) that are distributed using MCP and TCP. By inspecting Figure 3, we can intuitively conclude that the maximum allowable path loss is diverse when the GUEs are distributed using MCP and TCP. In Figure 3, we plot the CDFs for the cases when 50% and 97.5% of the MBS are destroyed. A close inspection of Figure 3 reveals that the variation in CDFs is minimum for the different numbers of UABSs deployed and for a different number of the MBSs destroyed. Both MCP and TCP observe a similar distribution in CDF, and the maximum allowable path loss for the system when the GUEs are distributed using both processes is approximately 240 dB.

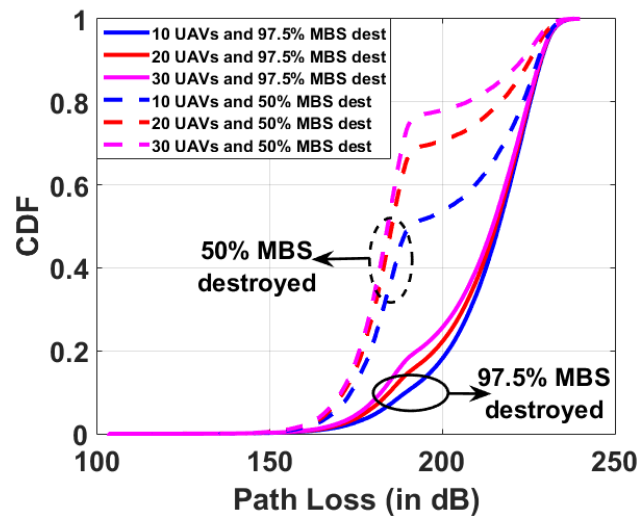


Figure 3. The CDF describes the combined path loss observed from all the base stations in PSC AG-HetNet. The dashed lines correspond to the scenario where 50% of the MBSs are destroyed, while solid lines correspond to the scenario with 97.5% of the MBSs being destroyed. The CDF is plotted for GUEs distribution using the Matern and Thomas clusters processes.

2.2. Inter-Cell Interference Considerations in the AG-HetNet

The small cells, such as the UABS shown in Figure 1, have low transmission power and a finite ability to schedule GUEs compared to MBSs. Therefore, we consider the positive-bias CRE technique defined in 3GPP Release-8 at UABS to extend the network coverage and increase the capacity by offloading GUEs from congested MBSs or consuming the unscheduled users. However, positive-bias CRE at UABS could potentially increase the interference at the GUEs located in the cell edge or expanded region. To address this interference introduced between the MBS-UABS cells, MBS can use the ICIC techniques defined in 3GPP Release-10/11 [4,5]. Using these ICIC techniques, MBSs can transmit radio frames at reduced power levels, of which an example frame is shown in Figure 4.

As seen in Figure 4, it illustrates an example of radio subframes for AG-HetNet, where frames with full transmit power are the uncoordinated subframes (USF) and subframes with reduced power as the coordinated subframes (CSF). We define α_* as the power reduction factor of radio subframes, and the power reduction factor at MBS is given by α_{mbs} . The range of the power reduction factor is given by $\alpha_{\text{mbs}} \in [0, 1]$, such that $\alpha_{\text{mbs}} = 0$ corresponds to the 3GPP Release-10 almost blank subframes (ABS) eICIC technique, $\alpha_{\text{mbs}} = 1$ corresponds to no ICIC, and otherwise, $0 < \alpha_{\text{mbs}} < 1$ corresponds to the reduced power FeICIC technique defined in 3GPP Release-11.

The reduced power FeICIC at MBSs aims at protecting specific UABS subframes from MBS, as seen in Figure 4. To regulate the duty cycle and coordinate the radio frames, we consider factor β_{mbs} and $(1 - \beta_{\text{mbs}})$ at MBS for USF and CSF, respectively. The public safety AG-HetNet's system design assumes the power reduction pattern, radio subframe duty cycle, and spectrum parameters to be shared via the X2 interface, which is a logical interface between the base stations.

The MBSs in the AG-HetNet greatly benefit from the application of ICIC techniques as it reduces the intercell interference into adjacent cells; however, ICIC also reduces the quality of service (QoS) at the scheduled GUEs. Therefore, to improve the QoS in the AG-HetNet, we consider the 3DBF technique at each transmitting base station to restrict the beamforming and power transmission at the location of scheduled GUEs [39].

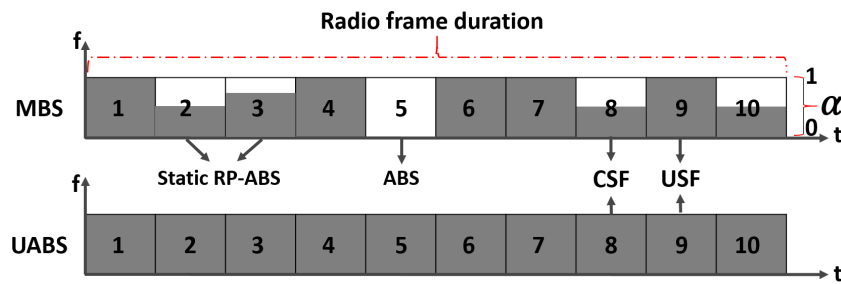


Figure 4. Illustration of LTE-Advanced frame structures for time-domain ICIC techniques, i.e., almost blank subframes (ABS) with $\alpha = 0$ is the 3GPP Release-10 eICIC, $0 < \alpha < 1$ is the reduced power, and ABS (RP-ABS) is the 3GPP Release-11 FeICIC.

2.3. Cell Selection, User Association, and Handover of GUEs in AG-HetNet

Using the familiarity with the system model defined so far, the ICIC interference mitigation techniques defined across all 3GPP Releases, and the design for reduced power CSF and USF specified in Figure 4, we define the SIR experienced by a n th arbitrary GUE scheduled in USF or CSF of the base stations of interest (MOI/UOI) by following an approach similar to that given in [4,5] and Table 3. Let $\Gamma_{\text{usf}}^{\text{mbs}}$, $\Gamma_{\text{csf}}^{\text{mbs}}$, $\Gamma_{\text{usf}}^{\text{uabs}}$, and $\Gamma_{\text{csf}}^{\text{uabs}}$ be the SIRs for the GUE scheduled in the CSF or USF radio subframes of the base station of interest (MOI/UOI). In Table 3, we define I_{agg} as the aggregate interference experienced at scheduled GUEs from all base stations except the base stations of interest (MOI or UOI).

The process of cell selection uses the SIR definition given in Table 3 for each base-stations of interest (MOI and UOI) and the positive-biased CRE τ_{uabs} at UABSs. The positive-biased CRE τ_{uabs} at UABSs is applied to increase the SIR coverage. Consequently, during a cell selection, the GUE always prefers camping on base stations of interest (i.e., MOI or UOI), which guarantees the most suitable SIR. After cell selection, an MBS-GUE (MUE) and UABS-GUE (UUE) would be scheduled in either USF or CSF radio subframes based on the scheduling threshold of ρ_{uabs} at UABS and ρ_{mbs} at MBS. This strategy of cell selection and GUE scheduling in USF or CSF subframes of base stations of interest (MOI or UOI) is similar to that of [4,5] and is summarized in Figure 5.

Once the n th arbitrary GUE is assigned to the base stations of interest (i.e., MOI or UOI) and scheduled in the USF or CSF radio subframe, using the SIR definitions, the Shannon capacity of the GUE scheduled in the CSF and USF subframes is defined by $C_{\text{usf}}^{\text{mbs}}$, $C_{\text{csf}}^{\text{mbs}}$, $C_{\text{usf}}^{\text{uabs}}$, and $C_{\text{csf}}^{\text{uabs}}$. In Table 3, $N_{\text{usf}}^{\text{uue}}$, $N_{\text{csf}}^{\text{uue}}$, $N_{\text{usf}}^{\text{mue}}$, and $N_{\text{csf}}^{\text{mue}}$ are the number of MUEs and UUEs scheduled in the USF or CSF subframes of the UABS and MBS, respectively.

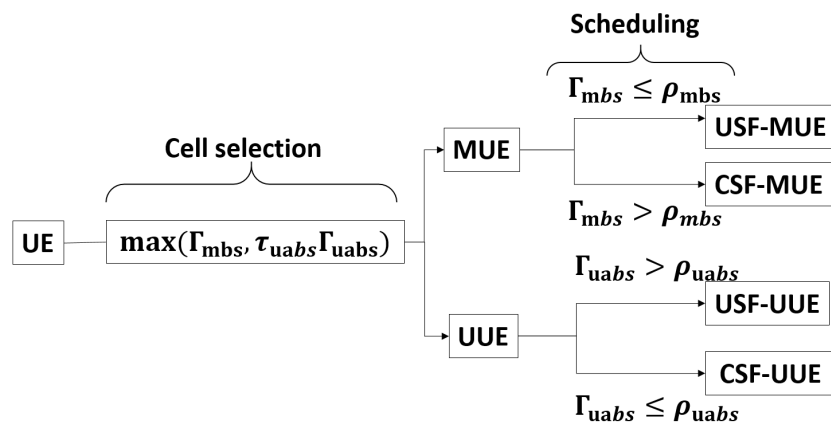


Figure 5. Cell selection, association, and handover of GUEs in coordinate and uncoordinated radio subframes for all base stations in the AG-HetNet.

Table 3. Shannon capacity definitions in terms of SIR and RSRP for USF/CSF radio frames.

SIR Ratio	Shannon Capacity of USF/CSF Radio Frames
$\Gamma_{\text{usf}}^{\text{mbs}} = \frac{R_{\text{uabs}}(d_{\text{un}})}{R_{\text{uabs}}(d_{\text{un}}) + I_{\text{agg}}}$	$C_{\text{usf}}^{\text{mbs}} = \frac{\beta_{\text{mbs}} \log_2(1 + \Gamma_{\text{usf}}^{\text{mbs}})}{N_{\text{usf}}^{\text{mbs}}}$
$\Gamma_{\text{csf}}^{\text{mbs}} = \frac{\alpha R_{\text{uabs}}(d_{\text{un}})}{R_{\text{uabs}}(d_{\text{un}}) + I_{\text{agg}}}$	$C_{\text{csf}}^{\text{mbs}} = \frac{(1 - \beta_{\text{mbs}}) \log_2(1 + \Gamma_{\text{csf}}^{\text{mbs}})}{N_{\text{csf}}^{\text{mbs}}}$
$\Gamma_{\text{usf}}^{\text{uabs}} = \frac{R_{\text{uabs}}(d_{\text{un}})}{R_{\text{mbs}}(d_{\text{un}}) + I_{\text{agg}}}$	$C_{\text{usf}}^{\text{uabs}} = \frac{(\beta_{\text{mbs}}) \log_2(1 + \Gamma_{\text{usf}}^{\text{uabs}})}{N_{\text{usf}}^{\text{uabs}}}$
$\Gamma_{\text{csf}}^{\text{uabs}} = \frac{R_{\text{uabs}}(d_{\text{un}})}{\alpha R_{\text{mbs}}(d_{\text{un}}) + I_{\text{agg}}}$	$C_{\text{csf}}^{\text{uabs}} = \frac{(1 - \beta_{\text{mbs}}) \log_2(1 + \Gamma_{\text{csf}}^{\text{uabs}})}{N_{\text{csf}}^{\text{uabs}}}$

3. UABS Placement and ICIC Parameter Optimization in AG-HetNet

The public safety scenario considered in Figure 2 with AG-HetNet can occur during a natural disaster such as a hurricane or earthquake. During such an event, the existing terrestrial infrastructure can receive severe damage and the remaining terrestrial infrastructure could see a surge in traffic. It would cause traffic congestion in the remaining commercial cellular networks and public safety networks. Thus, resulting in GUEs experiencing poor QoS and to address the lack of coverage in this scenario, the system design considers optimizing network parameters and maximizing the two KPIs. To this end, this simulative study is limited to investigating the gains using the *brute force algorithm*. For the AG-HetNet under consideration, the 5pSE corresponds to the worst fifth-percentile GUE capacity amongst all the scheduled GUEs, whereas the coverage probability of the AG-HetNet is defined as the percentage of the geographical area with broadband rates and a capacity larger than a threshold of $T_{\text{CSE}}^{\text{Shannon}}$.

Through each UABS $i \in \{1, 2, \dots, N_{\text{uabs}}\}$ in the AG-HetNet, we capture individual locations in (x_i, y_i) , where $\mathbf{L}_{\text{uabs}}^{\text{3D}}$ would be the matrix representing these locations in 3D. These UABSs are placed within the rectangular simulation area regardless of the existing MBS ($\mathbf{L}_{\text{mbs}}^{\text{3D}}$). Given the locations of the base station ($\mathbf{L}_{\text{uabs}}^{\text{3D}}$ and $\mathbf{L}_{\text{mbs}}^{\text{3D}}$), the matrix representation of individual ICIC parameters for each UABS is given by $\mathbf{S}_{\text{uabs}}^{\text{ICIC}} = [\boldsymbol{\tau}_{\text{uabs}}, \boldsymbol{\rho}_{\text{uabs}}] \in \mathbb{R}^{N_{\text{uabs}} \times 2}$. Similarly, the matrix representation of individual ICIC parameters for each MBS $\mathbf{S}_{\text{mbs}}^{\text{ICIC}} = [\boldsymbol{\alpha}_{\text{mbs}}, \boldsymbol{\beta}_{\text{mbs}}, \boldsymbol{\rho}_{\text{mbs}}] \in \mathbb{R}^{N_{\text{mbs}} \times 3}$.

We capture the resource management parameters in vectors, where $\boldsymbol{\rho}_{\text{mbs}} = [\rho_1, \dots, \rho_{N_{\text{mbs}}}]^T$ and $\boldsymbol{\rho}_{\text{uabs}} = [\rho_1, \dots, \rho_{N_{\text{uabs}}}]^T$ are the scheduling thresholds, respectively, for each MBS and UABS. The power reduction factor at each MBS is given by $\boldsymbol{\alpha}_{\text{mbs}} = [\alpha_1, \dots, \alpha_{N_{\text{mbs}}}]^T$, and $\boldsymbol{\beta}_{\text{mbs}} = [\beta_1, \dots, \beta_{N_{\text{mbs}}}]^T$ is the USF/CSF duty cycle for each MBS. Finally, the positive range expansion bias at each UABS is captured in $\boldsymbol{\tau}_{\text{uabs}} = [\tau_1, \dots, \tau_{N_{\text{uabs}}}]^T$. Using these vectors, the initial state of the public safety AG-HetNet under consideration can be given as $\mathbf{S} = [\mathbf{L}_{\text{uabs}}^{\text{3D}}, \mathbf{S}_{\text{mbs}}^{\text{ICIC}}, \mathbf{S}_{\text{uabs}}^{\text{ICIC}}]$.

In this simulative study, the upper bound, lower bound, and step size of these variables are defined in Table 4, where $\mathbb{D}\alpha_{\text{mbs}}, \mathbb{D}\beta_{\text{mbs}}, \mathbb{D}\rho_{\text{mbs}}, \mathbb{D}\rho_{\text{uabs}}, \mathbb{D}\tau_{\text{uabs}}, \mathbb{D}x$, and $\mathbb{D}y$ denote the step sizes for the $\alpha_{\text{mbs}}, \beta_{\text{mbs}}, \rho_{\text{mbs}}, \rho_{\text{uabs}}, \tau_{\text{uabs}}$, and x coordinate of a UABS's location and the y coordinate of a UABS's location, respectively. Whereas $\rho_{\text{mbs}}^{\text{low}}$ and $\rho_{\text{uabs}}^{\text{low}}$ denote the lower bounds for ρ_{mbs} and ρ_{uabs} , respectively. Similarly, $\rho_{\text{mbs}}^{\text{high}}$ and $\rho_{\text{uabs}}^{\text{high}}$ denote the upper bounds for ρ_{mbs} and ρ_{uabs} , respectively. This table shows that the Brute force algorithm must consider a large search space to find all feasible solutions. However, to lessen the system complexity and simulation runtime, we apply the same $\mathbf{S}_{\text{mbs}}^{\text{ICIC}}$ parameters across all MBSs and $\mathbf{S}_{\text{uabs}}^{\text{ICIC}}$ across all UABSs. Finally, we define the dependency of the 5pSE and coverage probability to the UABS locations, CRE, and ICIC parameters as

$$C_{5\text{pSE}}(\mathbf{L}_{\text{uabs}}^{\text{3D}}, \mathbf{S}_{\text{mbs}}^{\text{ICIC}}, \mathbf{S}_{\text{uabs}}^{\text{ICIC}}), \quad (7)$$

$$C_{\text{COV}}(\mathbf{L}_{\text{uabs}}^{\text{3D}}, \mathbf{S}_{\text{mbs}}^{\text{ICIC}}, \mathbf{S}_{\text{uabs}}^{\text{ICIC}}), C_{\text{COV}} > T_{\text{CSE}}^{\text{Shannon}}, \quad (8)$$

where $C_{5pSE}(\cdot)$ denotes the objective function for 5pSE, $C_{cov}(\cdot)$ denotes the objective function for coverage probability, and $T_{CSE}^{Shannon}$ is the capacity threshold supporting broadband rates. Using this definition of objective functions, the best state (\mathbf{BS}'_{KPI}) of all the possible states (\mathbf{S}) is given as

$$\mathbf{BS}'_{KPI} = \arg \max_{\mathbf{S}} C_{KPI}(\mathbf{S}), \quad (9)$$

where $C_{KPI}(\cdot)$ is a generic representation of the objective function defined in (7) and (8) and $\mathbf{KPI} \in (5pSE, COV)$.

Table 4. Boundary values and the step size of each parameter to be optimized within the search space.

Search Parameter	Parameter Range	Search Space Size
α_{mbs}	$0, \mathbb{D}\alpha_{mbs}, 2\mathbb{D}\alpha_{mbs}, \dots, 1$	$1/\mathbb{D}\alpha_{mbs} + 1$
β_{mbs}	$0, \mathbb{D}\beta_{mbs}, 2\mathbb{D}\beta_{mbs}, \dots, 1$	$1/\mathbb{D}\beta_{mbs} + 1$
ρ_{mbs}	$\rho_{mbs}^{low}, \rho_{mbs}^{low} + \mathbb{D}\rho_{mbs}, \rho_{mbs}^{low} + 2\mathbb{D}\rho_{mbs}, \dots, \rho_{mbs}^{high}$	$\frac{(\rho_{mbs}^{high} - \rho_{mbs}^{low})}{(\mathbb{D}\rho_{mbs})}$
ρ_{uabs}	$\rho_{uabs}^{low}, \rho_{uabs}^{low} + \mathbb{D}\rho_{uabs}, \rho_{uabs}^{low} + 2\mathbb{D}\rho_{uabs}, \dots, \rho_{uabs}^{high}$	$\frac{(\rho_{uabs}^{high} - \rho_{uabs}^{low})}{(\mathbb{D}\rho_{uabs})}$
τ_{uabs}	$0, \mathbb{D}\tau_{uabs}, 2\mathbb{D}\tau_{uabs}, \dots, \tau_{uabs}^{high}$	$\frac{\tau_{uabs}^{high}}{\mathbb{D}\tau_{uabs}}$
X coordinate of UABS	$-1/2, -1/2 + \mathbb{D}x, -1/2 + 2\mathbb{D}x, \dots, 1/2$	$\frac{1}{\mathbb{D}x}$
Y coordinate of UABS	$-1/2, -1/2 + \mathbb{D}y, -1/2 + 2\mathbb{D}y, \dots, 1/2$	$\frac{1}{\mathbb{D}y}$

For the proposed AG-HetNet, UABSs are initially deployed on fixed hexagonal locations within the simulation area (AR_{sim}) as shown in Figure 6. In Figure 6a, we illustrate the UABSs' deployment on the fixed hexagonal location when 50% of the MBSs are destroyed, and in Figure 6b, when 95% of the MBSs are destroyed. Each UABS sends its 2D location coordinates and the system-level resources allocation for a GUE to an edge server, and using the brute-force algorithm described in Algorithm 1, the two KPIs of the AG-HetNet will be determined at the edge server. The global maxima values of the best state (\mathbf{BS}'_{KPI}) of all the possible states \mathbf{S} can be vectorized into $\mathbf{BS}'_{KPI} = [\hat{\mathbf{L}}_{uabs}^{(hex)}, \mathbf{BS}'_{mbs}^{ICIC}, \mathbf{BS}'_{uabs}^{ICIC}]$.

Algorithm 1 Pseudocode for brute-force algorithm

```

1: procedure  $C_{KPI}(\hat{\mathbf{L}}_{uabs}^{(hex)}, \mathbf{S}_{pbs}^{ICIC}, \mathbf{S}_{uabs}^{ICIC})$ 
2:   KPI : 5pSECOV
3:   COV, 5pSE, Best state  $\mathbf{BS}' \leftarrow \text{NULL}$ 
4:   for all Values of State  $\mathbf{S}$  do
5:     Current 5pSE  $\leftarrow C_{5pSE}(\mathbf{S})$ 
6:     if Current 5pSE > 5pSE then
7:       5pSE  $\leftarrow$  Current 5pSE
8:        $\mathbf{BS} \leftarrow \mathbf{S}$ 
9:     end if
10:    Current COV  $\leftarrow C_{COV}(\mathbf{S})$ 
11:    if Current COV > COV then
12:      COV  $\leftarrow$  Current COV
13:       $\mathbf{BS} \leftarrow \mathbf{S}$ 
14:    end if
15:  end for
16:  Return 5pSE, COV, Best state  $\mathbf{BS}'$ 
17: end procedure

```

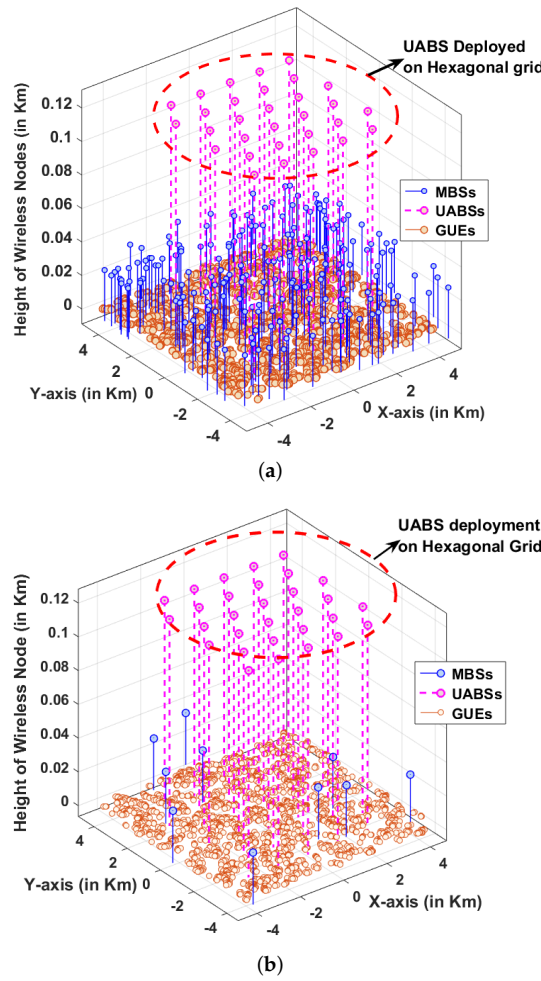


Figure 6. Illustration of PSC network after a disaster and UABSs deployed to restore mission-critical communications. (a) Illustration of PSC network after a disaster, with 50% of the infrastructure destroyed and UABSs deployed on a fixed hexagonal grid and at the height of 120 m. (b) Illustration of PSC network after a disaster, with 95% of the infrastructure destroyed and UABSs deployed on a fixed hexagonal grid and at the height of 120 m.

As a function of the step size and parameter range defined in Table 4, the time complexity for the brute-force algorithm and with UABS deployed on a fixed hexagonal grid is defined as

$$\mathcal{O}\left(\left(1/\mathbb{D}\alpha_{mbs} + 1\right) \times \left(1/\mathbb{D}\beta_{mbs} + 1\right) \times \left(\frac{\rho_{mbs}^{high} - \rho_{mbs}^{low}}{\mathbb{D}\rho_{mbs}}\right) \times \left(\frac{\tau_{pbs}^{high}}{\mathbb{D}\tau_{pbs}}\right) \times \left(\frac{\rho_{uabs}^{high} - \rho_{uabs}^{low}}{\mathbb{D}\rho_{uabs}}\right) \times \left(\frac{\tau_{uabs}^{high}}{\mathbb{D}\tau_{uabs}}\right)\right).$$

Lastly, a step-by-step articulation of the system design to system flow is given in Figure 7 using the system-level details discussed in Section 2, objective functions in Section 3, and brute force algorithms proposed in Algorithm 1. Furthermore, each step in the flow diagram refers to relevant figures, tables, and equations in the system design.

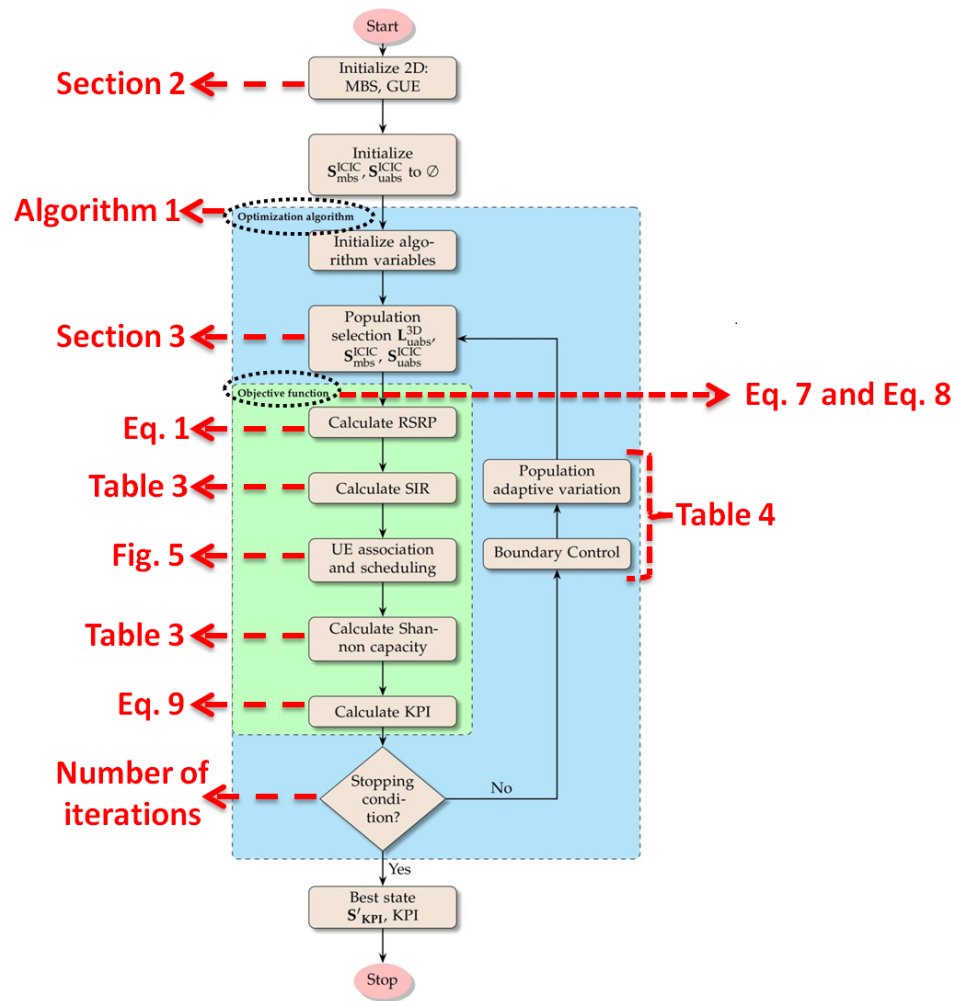


Figure 7. A flowchart combining AG-HetNet system flow and the Brute Force algorithm used.

4. Simulation Results and Discussion

In this section of the article, we compare and review the performance of the two KPIs for the public safety scenario illustrated in Figure 2, with/without ICIC techniques for the MCP and TCP distribution of GUEs, the different numbers of UABS deployment, and while considering a brute-force approach. We use Matlab-based computer simulation to define the brute force algorithm approach and objective functions. With extensive Monte Carlo simulation and design parameters set to the values given in Table 5, we calculate the KPIs of the wireless network, and for the obtained KPI values, we conduct a comparative study, and the following section discusses the same.

Table 5. System parameters and simulation values considered.

Parameter	Value
$A_{R_{sim}}$	100 km ²
$\Lambda_{mbs}, \Lambda_{gue}$	4 and 100 per km ²
N_{uabs}	10, 20, 30
Pow_{mbs}, Pow_{uabs}	46 and 30 dBm
h_{mbs}, h_{uabs}	36 and 120 m
h_{gue}	1.5 m
f_c^{B14}	763 MHz for downlink
α_{mbs}	0 to 1
β_{mbs}	0 to 100%
ρ_{mbs}	20 dB to 40 dB
ρ_{uabs}	-5 dB to 5 dB
τ_{uabs}	0 dB to 12 dB

4.1. KPI Evaluation and Optimization Using Brute Force

Aerial-HetNet performance when the 30, 20, and 10 number of UABSs are deployed on fixed hexagonal locations and at a fixed height is plotted in Figures 8 and 9. Subsequently, Figure 10 provides the performance comparison when GUEs are distributed using MCP. Similarly, when GUEs are distributed using TCP performance is plotted in Figures 11–13 provide the performance comparison. In particular, Figures 9 and 12 show the impact of positive-bias CRE at UABSs (along the x -axis) on the coverage probability (along the y -axis), whereas the performance of 5pSE (along the y -axis) and positive-bias CRE at UABSs (along the x -axis) can be seen in Figures 8 and 11 shows 5pSE. In an initial inspection of performance plots shown in Figures 8, 9, 11, and 12, we can intuitively conclude that FeICIC performs better when compared to eICIC and without any ICIC techniques when MBSs are 50% and 97.5% destroyed.

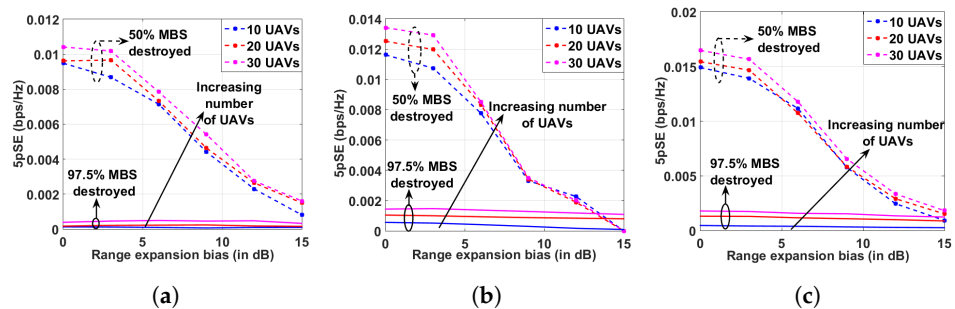


Figure 8. Peak 5pSE performance of the wireless network, when GUEs are distributed using MCP, UABS deployed on a fixed hexagonal grid, and for different ICIC techniques. (a) NIM Peak 5pSE vs. CRE. (b) eICIC Peak 5pSE vs. CRE. (c) FeICIC Peak 5pSE vs. CRE.

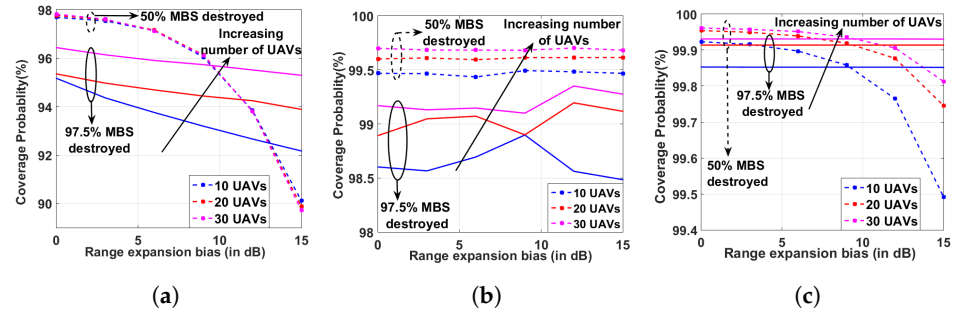


Figure 9. Peak coverage performance of the wireless network, when GUEs are distributed using MCP, UABS deployed on a fixed hexagonal grid, and for different ICIC techniques. (a) NIM Coverage probability vs. CRE. (b) eICIC Coverage probability vs. CRE. (c) FeICIC Coverage probability vs. CRE.

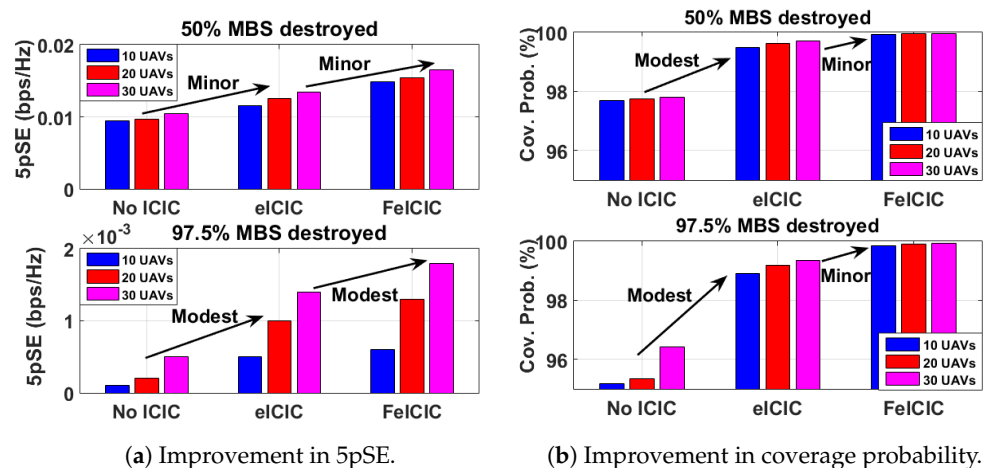


Figure 10. Performance comparison when GUEs are distributed using MCP and UABS deployed on a fixed hexagonal grid. (a) Improvement in 5pSE. (b) Improvement in coverage probability.

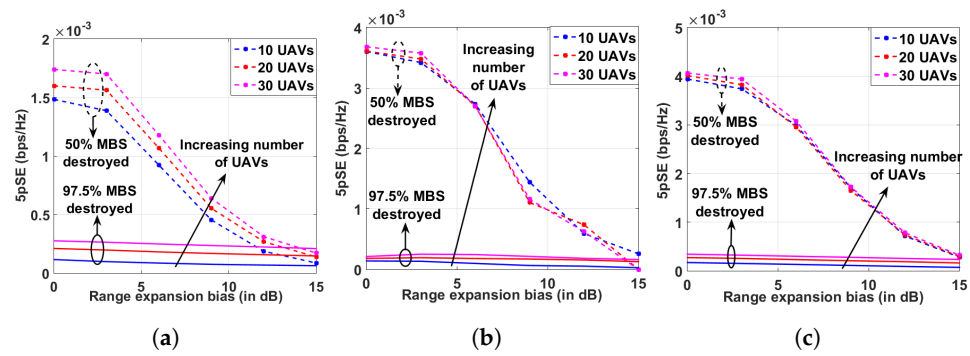


Figure 11. Peak 5pSE performance of the wireless network; when GUEs are distributed using TCP, UABS deployed on a fixed hexagonal grid, and for different ICIC techniques. (a) NIM Peak 5pSE vs. CRE. (b) eICIC Peak 5pSE vs. CRE. (c) FeICIC Peak 5pSE vs. CRE.

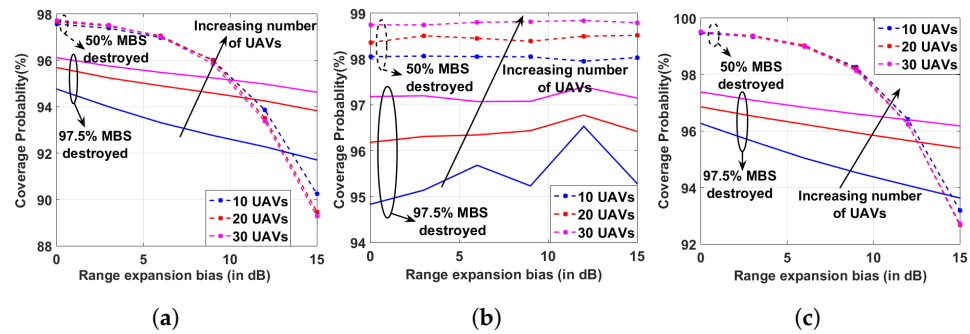


Figure 12. Peak coverage performance of the wireless network; when GUEs are distributed using TCP, UABS deployed on a fixed hexagonal grid, and for different ICIC techniques. (a) NIM Coverage probability vs. CRE. (b) eICIC Coverage probability vs. CRE. (c) FeICIC Coverage probability vs. CRE.

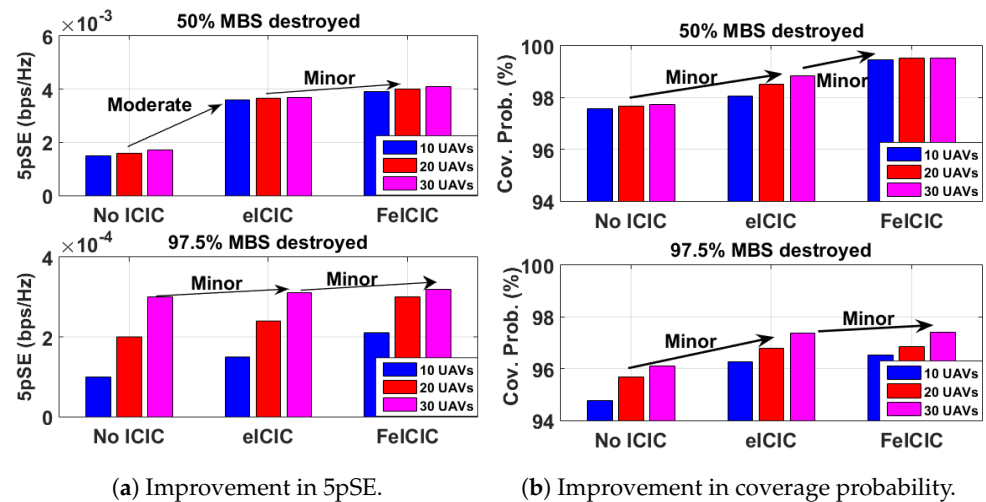


Figure 13. Performance comparison when GUEs are distributed using TCP and UABS deployed on a fixed hexagonal grid.

4.1.1. Performance Evaluation When GUEs Are Distributed Using MCP

For a varied number of UABS deployed in the AG-HetNet, we plot the 5pSE variation for a positive bias CRE as seen in Figure 8a–c. When 50% of the MBSs are destroyed, the peak values in the case of the no-ICIC mechanism (NIM), eICIC, and FeICIC observed lower values of CREs. Moreover, as the CRE increases, the number of GUEs associated with the UABSs increases, and so does the interference experienced by these GUEs, thus decreasing the overall 5pSE. In a high disaster-struck scenario, when 97.5% of the MBSs are destroyed, a relatively slow degradation of peak values of 5pSE is observed with the increasing CRE for NIM, eICIC, and FeICIC techniques.

In Figure 9a–c, we plot the coverage probability variation for a positive-biased CRE. When 50% of the MBSs are destroyed, the peak values of NIM, eICIC, and FeICIC are observed for the moderate values of positive-biased CREs. Moreover, as the CRE increases, the number of GUEs associated with the UABSs increases, and so does the interference experienced by these GUEs, thus decreasing the overall 5pSE. In a high disaster-struck scenario, when 97.5% of the MBSs are destroyed, the peak value of 5pSE for NIM is observed at around 0 dB CRE, the eICIC technique observes a peak value in the range of 10–12 dB CRE, and FeICIC is observed in the range of 0–3 dB CRE.

Following the comparative analysis of KPIs shown in Figure 10a,b, we observe a minor deviation in the peak values of 5pSE between NIM, eICIC, and FeICIC when 50% of MBSs are destroyed—a modest deviation in the peak values when 97.5% of MBSs are destroyed. In comparison, we observe a modest deviation in the peak values from NIM to eICIC and a minor deviation in the peak values from eICIC to FeICIC for coverage probability in both scenarios of 50% and 97.5% of the MBSs being destroyed.

4.1.2. Performance Evaluation When GUEs Are Distributed Using TCP

The AG-HetNet performance is outlined in Figure 11a–c; we plot the 5pSE variation with respect to positive-biased CRE. The result demonstrates that when 50% of the MBSs are destroyed, the peak values in the case of NIM, eICIC, and FeICIC are observed with lower values of CREs. Moreover, as the CRE increases, the number of GUEs associated with the UABSs increases, and so does the interference experienced by these GUEs, thus decreasing the overall 5pSE. In a high disaster-struck scenario, when 97.5% of the MBSs are destroyed, a relatively slow degradation of peak values of 5pSE is observed with the increasing CRE for the NIM, eICIC, and FeICIC ICIC techniques.

Similarly, we discuss the coverage probability variation for positive-biased CRE. The results in Figure 12a–c demonstrate that when 50% of the MBSs are destroyed, the peak values in the case of NIM, eICIC, and FeICIC are observed for the moderate values of CREs. Moreover, as the CRE increases, the number of GUEs associated with the UABSs increases, and so does the interference experienced by these GUEs, thus decreasing the overall 5pSE. Whereas in a high disaster-struck scenario with 97.5% of the MBSs destroyed, the peak value of 5pSE for NIM is observed in the range of 0–3 dB CRE, the eICIC technique observes a peak value around 12 dB CRE, and FeICIC is observed in the range of 0–3 dB CRE.

Following the comparative analysis of KPIs illustrated in Figure 13a,b for 5pSE, we observe a moderate deviation in the peak values from NIM to eICIC and a minor deviation in the peak values from eICIC to FeICIC when 50% of MBSs are destroyed. Furthermore, we observe a minor deviation in the peak values of 5pSE between NIM, eICIC, and FeICIC when 97.5% of MBSs are destroyed. In comparison, we observe a minor deviation in the peak coverage probability between NIM, eICIC, and FeICIC in both scenarios of 50% and 97.5% of the MBSs being destroyed.

4.2. Performance Comparison of the KPIs

Using the results given in Figures 8 and 11 and the KPI values captured in Tables 6–9, we summarize our critical results demonstrated in earlier simulations when using brute-force techniques with/without ICIC optimization for different clustered distributions of GUEs in AG-HetNet.

From the simulation results given in Figures 9 and 12, we observe reduced power FeICIC in Release-11, which is observed to outperform Release-10 eICIC and without any ICIC, in terms of the overall 5pSE and coverage probability of the AG-HetNet. Further inspection reveals that the peak values of 5pSE and coverage probability are observed when fewer MBSs are destroyed. Also, the 5pSE and coverage probability is higher when more UABSs are deployed.

Table 6. Coverage probability peak value observations in % and when GUEs are distributed using TCP distribution.

Brute Force Algorithm						
TCP Distribution						
MBSs destroyed	50%			97.5%		
No UABSs	10	20	30	10	20	30
NIM	97.6870	97.7613	97.8160	95.1673	95.3484	96.4353
eICIC	99.4927	99.6142	99.7019	98.8974	99.1949	99.3506
FeICIC	99.9231	99.9541	99.9544	99.8530	99.9140	99.9310

Table 7. Coverage probability peak value observations in % and when GUEs are distributed using MCP distribution.

Brute Force Algorithm						
MCP Distribution						
MBSs destroyed	50%			97.5%		
No UABSs	10	20	30	10	20	30
NIM	97.5664	97.6774	97.7281	94.7658	95.6932	96.1169
eICIC	98.0655	98.5168	98.8411	96.2666	96.7794	97.3837
FeICIC	99.4767	99.5146	99.5168	96.5326	96.8583	97.3923

Table 8. 5pSE peak value observations in bps/kHz and when GUEs are distributed using MCP distribution.

Brute Force Algorithm						
MCP Distribution						
MBSs destroyed	50%			97.5%		
No UABSs	10	20	30	10	20	30
NIM	0.0095	0.0097	0.0104	0.0001	0.0002	0.0003
eICIC	0.0116	0.0125	0.0134	0.0005	0.0010	0.0014
FeICIC	0.0149	0.0154	0.0165	0.0006	0.0013	0.0018

Table 9. 5pSE peak value observations in bps/kHz and when GUEs are distributed using TCP distribution.

Brute Force Algorithm						
TCP Distribution						
MBSs destroyed	50%			97.5%		
No UABSs	10	20	30	10	20	30
NIM	0.0015	0.0016	0.0017	0.0001	0.0002	0.0003
eICIC	0.0036	0.00365	0.0037	0.00015	0.00024	0.00031
FeICIC	0.0039	0.0040	0.0041	0.00021	0.00030	0.00032

Finally, we summarize the peak values observed for coverage probability and 5pSE for with/without ICIC techniques for different GUE distributions, while using brute force and UABS deployed on a fixed hexagonal grid is captured in Tables 6–9. We can see the improvement in performance as the AG-HetNet transitions from using NIM to eICIC to FeICIC. Furthermore, we can also see the improvement with the increasing number of UABSs deployed. Even though the number of UABSs increases the probability of inter-cell interference, this interference is mitigated using techniques considered in the system model, such as the 3DBF and ICIC management techniques.

4.3. Future Work

In this article, we established a system design and definitions for the AG-HetNet public safety network while considering the impact of real-life disasters such as hurricanes or earthquakes. However, we limited the scope of the initial investigation to simply a

performance evaluation of the wireless network. Thus, in the future, critical aspects under consideration include

- Considering the UABS deployment's height variation and mobility in the coordinate system. However, as the deployment height increases, LOS also increases and, in turn, increases the interference at the users located in the cell edge or in the range-expanded regions of small cells. The future system model would be tuned to consider this impact of LOS and interference.
- Considering a multi-tier AG-HetNet with fixed terrestrial cells such as macro-cells and pico-cells and UABSs as aerial small-cells.
- Determining suitable machine learning algorithms for achieving the best performance of the AG-HetNet. However, the complexity of simulating any machine learning algorithm depends on the optimization dimension, the population size, and the cost of the objective function. Therefore, also define a strategy for joint optimization of the wireless network resource scheduling and UABS placement while evaluating the KPIs.

5. Conclusions

In this article, concerning a geographical area struck with high disaster, we simulate and demonstrate the UABS's capabilities to maintain and restore mission-critical communications in the event of any damage to the public safety infrastructure. Through Monte Carlo simulations, we maximized the coverage probability and 5pSE gains of the overall AG-HetNet, while mitigating intercell interference and optimizing the ICIC parameters. Furthermore, we compare and analyze the 5pSE and coverage probability of the AG-HetNet for different GUEs' distribution when UABSs are deployed on a fixed hexagonal grid and different numbers of UABS are deployed. The result outlines that the AG-HetNets with reduced power subframes (FeICIC) yield better 5pSE than almost blank subframes (eICIC).

Funding: This research received no specific grant from any funding agency in the public, commercial, or not-for-profit sectors.

Data Availability Statement: Data are contained within the article.

Conflicts of Interest: The author declares no conflict of interest. Author Abhaykumar Kumbhar was employed by the company Motorola Solutions, Inc.

Abbreviations

The following abbreviations are used in this manuscript:

3DBF	Three-dimension beam forming
5pSE	Fifth-percentile spectral efficiency
ABS	Almost blank subframes
AG-HetNet	Air-ground heterogeneous cellular network
CRE	Cell range expansion
CSF	Coordinated radio-subframes
eICIC	Enhanced intercell interference coordination
FeICIC	Further-enhanced intercell interference coordination
GUE	Ground user equipment
HetNet	Heterogeneous network
ICIC	Intercell interference coordination
LOS	Line of sight
LTE	Long term evolution
MBS	Macro base-stations
MCP	Matérn cluster process
MOI	MBS cell-of-interest
MUE	MBS GUE
NIM	No interference management

NLOS	Non line of sight
OHPLM	Okumara–Hata path loss model
PSC	Public safety communications
QoS	Quality of service
RP-ABS	Reduce power almost blank subframes
RSRP	Reference symbol received power
SE	Spectral Efficiency
SIR	Signal-to-interference ratio
TCP	Thomas cluster process
UAV	Unmanned aerial vehicle
UABS	Unmanned aerial base-stations
UE	User equipment
UOI	UABS cell-of-interest
USF	Uncoordinated radio-subframes
UUE	UABS GUE

References

- Han, S.I. Survey on UAV deployment and trajectory in wireless communication networks: Applications and challenges. *Information* **2022**, *13*, 389. [\[CrossRef\]](#)
- Kumbhar, A.; Koohifar, F.; Guvenc, I.; Mueller, B. A survey on legacy and emerging technologies for public safety communications. *IEEE Commun. Survery Tutor.* **2016**, *18*, 97–124. [\[CrossRef\]](#)
- Chandrasekharan, S.; Gomez, K.; Al-Hourani, A.; Kandeepan, S.; Rasheed, T.; Goratti, L.; Reynaud, L.; Grace, D.; Bucaille, I.; Wirth, T.; et al. Designing and implementing future aerial communication networks. *IEEE Commun. Mag.* **2016**, *54*, 26–34. [\[CrossRef\]](#)
- Kumbhar, A.; Binol, H.; Singh, S.; Güvenç, İ.; Akkaya, K. Heuristic approach for jointly optimising FeICIC and UAV locations in multi-tier LTE-advanced public safety HetNet. *IET Commun.* **2020**, *14*, 3585–3598. [\[CrossRef\]](#)
- Kumbhar, A.; Güvenç, İ.; Singh, S.; Tuncer, A. Exploiting LTE-Advanced HetNets and FeICIC for UAV-assisted public safety communications. *IEEE Access* **2018**, *6*, 783–796. [\[CrossRef\]](#)
- AT&T. *Flying COW Connects Puerto Rico*; Technical Report; AT&T: Dallas, TX, USA, 2017.
- The Drive. *AT&T and Verizon Test 4G LTE Drones in New Jersey*; Technical Report; The Drive: New York, NY, USA, 2018.
- CNBC. *AT&T and Verizon Drones Provide Cell Service in Natural Disasters*; Technical Report; CNBC: Englewood Cliffs, NJ, USA, 2018.
- Federal Communications Commission (FCC). *WT Docket 06-150, PS Docket 06-229, and WP Docket No. 07-100. In the Matter of Service Rules for the 698–746. 747–762 and 777–792 MHz Bands. Implementing a Nationwide, Broadband, Interoperable Public Safety Network in the 700 MHz Band. Amendment of Part 90 of the Commission’s Rules*; Federal Communications Commission (FCC): Washington, DC, USA, 2011.
- Aynew, T.M.; Xenakis, D.; Passas, N.; Merakos, L. A Novel Content Placement Strategy for Heterogeneous Cellular Networks with Small Cells. *IEEE Netw. Lett.* **2019**, *2*, 10–13. [\[CrossRef\]](#)
- Gibbs, C. Verizon claims largest small cell deployment in the U.S. Technical Report. *Fierce Wirel.* **2017**.
- Heisler, Y. AT&T wants to use drones to improve its LTE network. Technical Report. *Yahoo Tech News*, 16 June 2016.
- Nakamura, T.; Nagata, S.; Benjebbour, A.; Kishiyama, Y.; Hai, T.; Xiaodong, S.; Ning, Y.; Nan, L. Trends in small cell enhancements in LTE advanced. *IEEE Commun. Mag.* **2013**, *51*, 98–105. [\[CrossRef\]](#)
- Al-Kadri, M.O.; Deng, Y.; Aijaz, A.; Nallanathan, A. Full-Duplex Small Cells for Next Generation Heterogeneous Cellular Networks: A Case Study of Outage and Rate Coverage Analysis. *IEEE Access* **2017**, *5*, 8025–8038. [\[CrossRef\]](#)
- Turgut, E.; Gursoy, M.C. Downlink Analysis in Unmanned Aerial Vehicle (UAV) Assisted Cellular Networks with Clustered Users. *IEEE Access* **2018**, *6*, 36313–36324. [\[CrossRef\]](#)
- Azari, M.M.; Rosas, F.; Chiumento, A.; Pollin, S. Coexistence of terrestrial and aerial users in cellular networks. In Proceedings of the IEEE Global Communications Conference 2017, Singapore, 4–8 December 2017; pp. 1–6.
- Singh, S.; Kumbhar, A.; Güvenç, İ.; Sichitiu, M.L. Intelligent Interference Management in UAV-Based HetNets. *Telecom* **2021**, *2*, 472–488. [\[CrossRef\]](#)
- Hayajneh, A.M.; Zaidi, S.A.R.; McLernon, D.C.; Di Renzo, M.; Ghogho, M. Performance analysis of UAV enabled disaster recovery networks: A stochastic geometric framework based on cluster processes. *IEEE Access* **2018**, *6*, 26215–26230. [\[CrossRef\]](#)
- Wang, Q.; Li, W.; Yu, Z.; Abbasi, Q.; Imran, M.; Ansari, S.; Sambo, Y.; Wu, L.; Li, Q.; Zhu, T. An Overview of Emergency Communication Networks. *Remote Sens.* **2023**, *15*, 1595. [\[CrossRef\]](#)
- Do-Duy, T.; Nguyen, L.D.; Duong, T.Q.; Khosravirad, S.R.; Claussen, H. Joint optimisation of real-time deployment and resource allocation for UAV-aided disaster emergency communications. *IEEE J. Sel. Areas Commun.* **2021**, *39*, 3411–3424. [\[CrossRef\]](#)
- Qi, Z.; Lahuerta-Lavieja, A.; Li, J.; Nagalapur, K.K. Deployable networks for public safety in 5G and beyond: A coverage and interference study. In Proceedings of the IEEE 4th 5G World Forum (5GWF), Montreal, QC, Canada, 13–15 October 2021; pp. 346–351.

22. Minhas, H.I.; Ahmad, R.; Ahmed, W.; Waheed, M.; Alam, M.M.; Gul, S.T. A reinforcement learning routing protocol for UAV aided public safety networks. *Sensors* **2021**, *21*, 4121. [[CrossRef](#)]
23. Waheed, M.; Ahmad, R.; Ahmed, W.; Mahtab Alam, M.; Magarini, M. On coverage of critical nodes in UAV-assisted emergency networks. *Sensors* **2023**, *23*, 1586. [[CrossRef](#)]
24. Wang, C.; Deng, D.; Xu, L.; Wang, W. Resource scheduling based on deep reinforcement learning in UAV assisted emergency communication networks. *IEEE Trans. Commun.* **2022**, *70*, 3834–3848. [[CrossRef](#)]
25. Deb, S.; Monogioudis, P.; Miernik, J.; Seymour, J.P. Algorithms for enhanced inter-cell interference coordination (eICIC) in LTE HetNets. *IEEE/ACM Trans. Netw.* **2014**, *22*, 137–150. [[CrossRef](#)]
26. Merwaday, A.; Mukherjee, S.; Güvenç, I. Capacity analysis of LTE-Advanced HetNets with reduced power subframes and range expansion. *EURASIP J. Wirel. Commun. Netw.* **2014**, *2014*, 1–19. [[CrossRef](#)]
27. Mukherjee, S.; Güvenç, I. Effects of range expansion and interference coordination on capacity and fairness in heterogeneous networks. In Proceedings of the IEEE Asilomar Conference Signals, Systems and Computers, Pacific Grove, CA, USA, 6–9 November 2011; pp. 1855–1859.
28. Kumbhar, A.; Güvenç, I. 3D Unmanned Aerial Vehicle Placement for Public Safety Communications. In *Springer Intelligent Unmanned Air Vehicles Communications for Public Safety Networks*; Springer: Berlin/Heidelberg, Germany, 2022; pp. 51–89.
29. Ahmad, I.; Hussain, S.; Mahmood, S.N.; Mostafa, H.; Alkhayyat, A.; Marey, M.; Abbas, A.H.; Abdulateef Rashed, Z. Co-Channel Interference Management for Heterogeneous Networks Using Deep Learning Approach. *Information* **2023**, *14*, 139. [[CrossRef](#)]
30. Tang, J.; Liu, G.; Pan, Q. A review on representative swarm intelligence algorithms for solving optimization problems: Applications and trends. *IEEE/CAA J. Autom. Sin.* **2021**, *8*, 1627–1643. [[CrossRef](#)]
31. Tang, J.; Chen, X.; Zhu, X.; Zhu, F. Dynamic reallocation model of multiple unmanned aerial vehicle tasks in emergent adjustment scenarios. *IEEE Trans. Aerosp. Electron. Syst.* **2022**, *59*, 1139–1155. [[CrossRef](#)]
32. Merwaday, A.; Tuncer, A.; Kumbhar, A.; Guvenc, I. Improved Throughput Coverage in Natural Disasters: Unmanned Aerial Base Stations for Public-Safety Communications. *IEEE Veh. Technol. Mag.* **2016**, *11*, 53–60. [[CrossRef](#)]
33. Afshang, M.; Saha, C.; Dhillon, H.S. Nearest-neighbor and contact distance distributions for Thomas cluster process. *IEEE Wirel. Commun. Lett.* **2016**, *6*, 130–133. [[CrossRef](#)]
34. Afshang, M.; Saha, C.; Dhillon, H.S. Nearest-neighbor and contact distance distributions for Matérn cluster process. *IEEE Commun. Lett.* **2017**, *21*, 2686–2689. [[CrossRef](#)]
35. Afshang, M.; Dhillon, H.S. Poisson cluster process based analysis of HetNets with correlated user and base station locations. *IEEE Trans. Wirel. Commun.* **2018**, *17*, 2417–2431. [[CrossRef](#)]
36. Saha, C.; Afshang, M.; Dhillon, H.S. 3GPP-inspired HetNet model using Poisson cluster process: Sum-product functionals and downlink coverage. *IEEE Trans. Commun.* **2017**, *66*, 2219–2234. [[CrossRef](#)]
37. Chun, Y.J.; Hasna, M.O.; Ghayeb, A.; Di Renzo, M. On modeling heterogeneous wireless networks using non-Poisson point processes. *arXiv* **2015**, arXiv:1506.06296.
38. 3GPP . Study on 3D Channel Model for LTE (Release 12). Technical Specification Group Radio Access Network, 3rd Generation Partnership Project (3GPP). Version 12.7.0. 1 May 2018, 36.873. Available online: <https://portal.3gpp.org/desktopmodules/Specifications/SpecificationDetails.aspx?specificationId=2574> (accessed on 2 August 2023).
39. Kammoun, A.; Khanfir, H.; Altman, Z.; Debbah, M.; Kamoun, M. Preliminary results on 3D channel modeling: From theory to standard. *IEEE J. Sel. Areas Commun. (JSAC)* **2014**, *32*, 1219–1229. [[CrossRef](#)]

Disclaimer/Publisher’s Note: The statements, opinions and data contained in all publications are solely those of the individual author(s) and contributor(s) and not of MDPI and/or the editor(s). MDPI and/or the editor(s) disclaim responsibility for any injury to people or property resulting from any ideas, methods, instructions or products referred to in the content.